

Schottky barriers at metal-finite semiconducting carbon nanotube interfaces

Yongqiang Xue * and Mark A. Ratner

Department of Chemistry and Materials Research Center, Northwestern University, Evanston, IL 60208

(Dated: October 29, 2018)

Electronic properties of metal-finite semiconducting carbon nanotube interfaces are studied as a function of the nanotube length using a self-consistent tight-binding theory. We find that the shape of the potential barrier depends on the long-range tail of the charge transfer, leading to an injection barrier thickness comparable to half of the nanotube length until the nanotube reaches the bulk limit. The conductance of the nanotube junction shows a transition from tunneling to thermally-activated transport with increasing nanotube length.

Single-wall carbon nanotubes (SWNT) are ideal systems for studying transport in the length scale ranging from the molecular limit as all-carbon cylindrical molecules to the bulk limit as quasi-one-dimensional conductors,¹ and many device concepts have been successfully demonstrated on a single-tube basis.^{2,3,4} Among the device physics problems raised, the nature of the electronic transport through a metal-semiconducting carbon nanotube interface stands out^{5,6,7,8} as one of the basic device building blocks.⁹ Although transport through a metal-long carbon nanotube interface has been studied using the bulk band structure and one-dimensional electrostatics,^{6,7,8} it is important to investigate device functionality of finite carbon nanotubes with lengths of nanometer range and three-dimensional electrostatics, which will also shed light on the scaling limit of carbon nanotube devices.

Here, we analyze the evolution of the electronic properties of the metal-finite SWNT interface as the length is varied from the molecular to the bulk limit. The model system is illustrated schematically in Fig. 1, where the open-ended SWNT molecule is attached to the surfaces of the metallic electrodes through the dangling bonds at the end. The device structure chosen represents an atomic-scale analogue of the metal-semiconductor interface since both the interface area and the active device region are atomic-scale. We find that the shape of the potential barrier depends on the charge transfer throughout the junction, which leads to an injection barrier thickness comparable to half of the nanotube length until the nanotube reaches the bulk limit. As a consequence, the SWNT junction conductance shows a transition from tunneling to thermally-activated transport as the nanotube length increases.

We take (10,0) SWNT as the prototype semiconducting SWNT, whose work function is taken as that of the graphite (4.5 eV).² We consider gold (Au) and titanium (Ti) electrodes as examples of high- and low- work function metals (5.1 and 4.33 eV respectively for polycrystalline materials). We describe the electronic structure of the isolated SWNT using the Extended Huckel Theory (EHT) with non-orthogonal basis sets $\phi_m(\vec{r})$,¹³ which gives a bulk (infinitely long) band gap of ≈ 0.9 eV for (10,0) SWNT. Since the SWNT Fermi level is located approximately at mid-gap, before the contact formation, the gold Fermi-level (-5.1 eV) lies below the valence

band edge while the titanium Fermi-level (-4.33 eV) lies between the mid-gap and conduction band edge of the bulk SWNT.

Since the screening of Coulomb interaction is relatively ineffective within the SWNT due to the reduced dimensionality,^{6,7} an atomistic study of the electronic processes throughout the metal-SWNT-metal junction is needed. We use a self-consistent tight-binding theory based on the semi-empirical implementation of the self-consistent Matrix Green's function (SCMGF) method for first-principles modeling of molecular-scale devices.¹⁰ Given the EHT Hamiltonian H_0 of the isolated SWNT, we calculate the density matrix ρ_{ij} and therefore the electron density of the equilibrium SWNT junction from

$$G^R = \{(E + i0^+)S - H - \Sigma_L(E) - \Sigma_R(E)\}^{-1}, \quad (1)$$

$$\rho = \int \frac{dE}{2\pi} \text{Imag}[G^R](E) f(E - E_F). \quad (2)$$

where the effect of coupling to the electrodes are included as matrix self-energy operators $\Sigma_{L(R)}$ and calculated using tight-binding parameters (we use a nanotube end-surface distance of 2.5 Å here).^{10,11} Here S is overlap matrix and $f(E - E_F)$ is the Fermi distribution describing the electrodes (see Ref. 10 for details). The SWNT Hamiltonian is now $H = H_0 + \delta V[\delta\rho]$ where $\delta\rho$ is the density of transferred charge and δV is the induced change in the electrostatic potential.

To proceed with self-consistent calculation, we approximate the charge distribution as superposition of atom-centered charge distributions¹² $\delta\rho(\vec{r}) = \sum_i \delta N_i \rho_i(\vec{r} - \vec{r}_i)$, where $\delta N_i = (\rho S)_{ii} - N_i^0$ and N_i^0 is the number of valence electrons on atomic-site i of the bare SWNT. $\rho_i(\vec{r}) = \frac{1}{N_{\zeta_i}} e^{-\zeta_i r}$ is a normalized Slater-type function ($\int d\vec{r} \rho_i(\vec{r}) = 1$).¹² The exponent ζ_i is chosen such that $\int d\vec{r} d\vec{r}' \rho_i(\vec{r}) \rho_i(\vec{r}') / |\vec{r} - \vec{r}'| = I_i - A_i$ ¹², where I_i (A_i) are the atomic electron affinity (ionization potential). In this way, we obtain $\delta V(\vec{r}) = \sum_i \delta N_i V_i(\vec{r} - \vec{r}_i)$, where $V_i = \int d\vec{r}' \rho_i(\vec{r}' - \vec{r}_i) / |\vec{r} - \vec{r}'|$ can be evaluated analytically¹². We take into account the image-potential effect by including within $\delta\rho$ both the transferred-charge on the carbon atoms and their image charges, rather than imposing an image-type potential correction. The matrix elements of the potential $\delta V_{mn} = \int d\vec{r} \phi_m^*(\vec{r}) \delta V(\vec{r}) \phi_n(\vec{r})$ are calculated using two types of scheme: (1) If m, n belong to the same atomic site i , we calculate it by direct numerical in-

tegration; (2) if m, n belong to different atomic sites, we use the approximation $\delta V_{mn} = S_{mn}(\delta V_{mm} + \delta V_{nn})/2$.

The finite SWNT lengths investigated are 2.0, 4.1, 8.4, 12.6, 16.9, 21.2 and 25.4 (nm), which corresponds to number of unitcells of 5, 10, 20, 30, 40, 50 and 60 respectively and spans the entire range from the molecular limit to the bulk limit. Due to the dangling bonds at the end, charge transfer occurs between the end and the interior carbon atoms of the SWNT, which should be corrected self-consistently first and give the initial charge configuration N_i^0 .¹⁰ The calculated charge transfer and electrostatic potential change for the Au-SWNT-Au and Ti-SWNT-Ti junctions are shown in Fig. 2. The magnified view of the transferred charge and potential shift at the interface and in the middle of the SWNT appear in Fig. 3.

The charge transfer at the metal-SWNT interface reflects the bonding configuration change upon contact to the metallic surfaces, involving mainly the end carbon atoms and decaying rapidly into the interior of the SWNT molecule.¹⁰ The electrostatic potential change is instead determined by the transferred charge throughout the metal-SWNT-junction due to the long-range Coulomb interaction, so its magnitude in the middle of the SWNT increases with increasing length until the finite SWNT reaches the bulk limit despite the small magnitude of the transferred charge in the middle of the SWNT.¹⁴ This gives a maximal barrier thickness for electron injection of roughly $10(nm)$, i.e., half of the nanotube length where it reaches the bulk limit (50 unitcells). The magnitude of both the charge transfer and the potential shift at the metal-SWNT interface are approximately the same for all the finite SWNTs studied.

For the SWNT molecules which have approached the bulk limit, the interface perturbation of the electron states in the middle can be essentially neglected. Charging and “band” shift is determined by the shift of the local density of states (LDOS) in the middle of the SWNT relative to the metal Fermi-level. Note that due to the three-dimensional electrostatics of the metal-SWNT-metal junction, the change in the electrostatic potential energy induced by the transferred charge decays moving away from the cylindrical surface of the SWNT. Therefore *the shift of the LDOS along the SWNT axis doesn't follow the shift in the potential energy*, different from the bulk metal-semiconductor interface. For the 60-unitcell SWNT, we find that for the Au-SWNT-Au junction the Fermi-level is located slightly below (by $\sim 0.05\text{eV}$) the mid-gap, while for the Ti-SWNT-Ti junction it is located above (by $\sim 0.15\text{eV}$) the mid-gap. This is consistent with the fact that in the interior of the SWNT the Fermi-level must lie within the band gap to ensure the small perturbation of the electron states there.

These charge transfer processes are often characterized as “charge-transfer doping”. For the Au-SWNT-Au (Ti-SWNT-Ti) junction, there is a small positive (negative) charge transfer of 5.7×10^{-4} (-6.4×10^{-5}) per atom in the middle of the 60-unitcell SWNT. The oscillation

of transferred-charge in the middle of the SWNT is due to the two-sublattice structure of zigzag tube, leading to charge transfer among atoms within the unitcell. The SWNT is therefore “hole-doped” by contacting to high work function (Au) and “electron-doped” by contacting to low work function (Ti) electrode. However, within the coherent transport regime, it is clear that both the charge transfer at the interface and the charge transfer inside the SWNT contribute only indirectly to electron transport by modulating the potential landscape across the metal-SWNT-metal junction.

Given the potential shift across the metal-SWNT interface, we can evaluate the length and temperature dependence of the SWNT junction conductance using the Landauer formula

$$G = \frac{2e^2}{h} \int dET(E) \left[-\frac{df}{dE}(E - E_F) \right] = G_{Tu} + G_{Th} \quad (3)$$

where the transmission is calculated from $T(E) = Tr[\Gamma_L(E)G^R(E)\Gamma_R(E)G^A(E)]$.¹⁰ Here we have separated the conductance into tunneling contribution $G_{Tu} = \frac{2e^2}{h}T(E_F)$ and thermal-activation contribution $G_{Th} = G - G_{Tu}$. The result for room temperature conductance is shown in Fig. 4. The tunneling conductance (also the zero temperature conductance) for both junctions decreases exponentially with the SWNT length for SWNT longer than 4.1(nm) appropriate for tunneling transport though potential barriers with identical barrier height. The room-temperature conductance instead saturates with increasing SWNT length. This is because the tunneling is exponentially suppressed for the longer SWNT molecules, while the transport becomes dominated by thermal-activation over the top of the potential barrier, whose height is approximately the same for all the finite SWNTs investigated. For Ti-SWNT-Ti junction, this leads to a transition from tunneling to thermally-activated transport at roughly $5(nm)$. For Au-SWNT-Au junction, the thermal contribution is already larger than the tunneling contribution for the smallest SWNT studied at room temperature.

The long-range nature of the charge transfer and potential barrier suggests the gate-modulation of junction conductance in SWNT-based transistors may be achieved through the modulation of the injection barrier at the metal-nanotube interface, in agreement with recent experimental works.⁴ The SWNT junction transport characteristics are sensitive to the shape of the potential change induced by both the gate voltage and source-drain voltage, whose effect increases with increasing SWNT length. Further analysis are needed to achieve a through understanding of nanotube-based devices.

This work was supported by the DARPA Moelectronics program, the DoD-DURINT program and the NSF Nanotechnology Initiative.

-
- * Corresponding author. Email: ayxue@chem.nwu.edu
- ¹ C. Dekker, *Phys. Today* **52**(5), 22 (1999).
 - ² S.J. Tans, A.R.M. Vershueren and C. Dekker, *Nature* **393**, 49 (1998); A. Bachtold, P. Hadley, T. Nakanishi and C. Dekker, *Science* **294**, 1317 (2001).
 - ³ T. Rueckes, K. Kim, E. Joslevich, G. Tseng, C. Cheung and C.M. Lieber, *Science* **289**, 94 (2000).
 - ⁴ V. Derycke, R. Martel, J. Appenzeller and Ph. Avouris, *Appl. Phys. Lett.* **80**, 2773 (2002); S. Heinze, J. Tersoff, R. Martel, V. Derycke, J. Appenzeller and Ph. Avouris, *Phys. Rev. Lett.* **89**, 106801 (2002).
 - ⁵ Y. Xue and S. Datta, *Phys. Rev. Lett.* **83**, 4844 (1999).
 - ⁶ F. Léonard and J. Tersoff, *Phys. Rev. Lett.* **84**, 4693 (2000); *Appl. Phys. Lett.* **81**, 4835 (2002).
 - ⁷ A.A. Odinson, *Phys. Rev. Lett.* **85**, 150 (2000).
 - ⁸ T. Nakanishi, A. Bachtold and C. Dekker, *Phys. Rev. B* **66**, 73307 (2002).
 - ⁹ E.H. Rhoderick and R.H. Williams, *Metal-Semiconductor Contacts*, 2nd edition (Clarendon Press, Oxford, 1988).
 - ¹⁰ Y. Xue, S. Datta and M. A. Ratner, *Chem. Phys.* **281**, 151 (2002); Y. Xue and M.A. Ratner, *MRS Proceedings* **734**, B6.8 (2003); cond-mat/0303179.
 - ¹¹ D. A. Papaconstantopoulos, *Handbook of the Band Structure of Elemental Solids* (Plenum Press, New York, 1986).
 - ¹² M. Elstner, D. Porezag, G. Jungnickel, J. Elsner, M. Haugk, Th. Frauenheim, S. Suhai and G. Seifert, *Phys. Rev. B* **58**, 7260 (1998).
 - ¹³ R. Hoffmann, *Rev. Mod. Phys.* **60**, 601 (1988); A. Rochefort, D.R. Salahub and Ph. Avouris, *J. Phys. Chem. B* **103**, 641 (1999).
 - ¹⁴ A quantum capacitance of ~ 0.3 pF/cm for the SWNT can be estimated from the differences in the potential change and transferred charge in the middle of the 50- and 60-unitcell SWNTs.

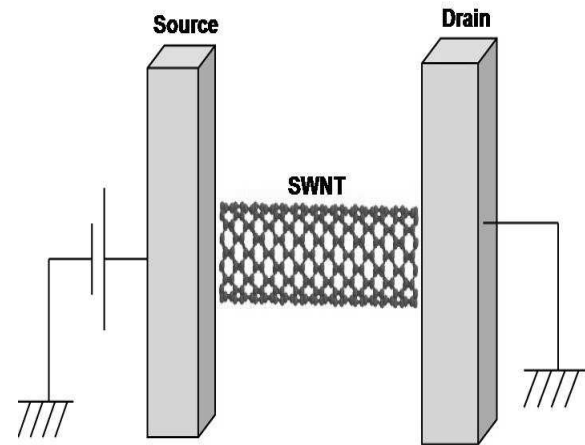


FIG. 1: Schematic illustration of the metal-SWNT-metal junction.

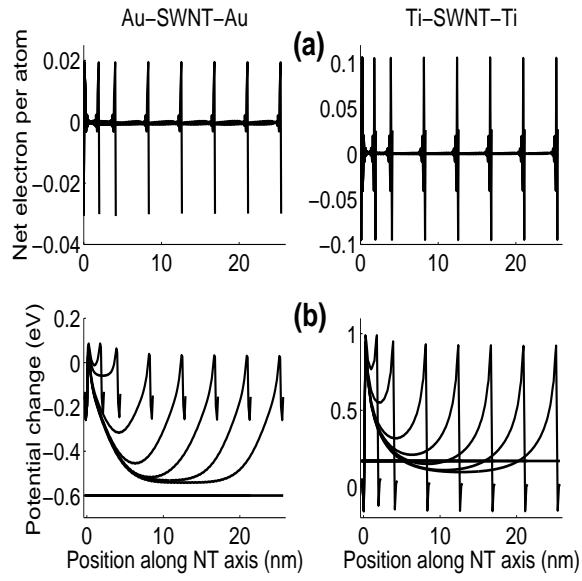


FIG. 2: Charge transfer (a) and electrostatic potential change (b) at the metal-finite SWNT-metal junction as a function of SWNT length for seven different lengths. The horizontal lines in (b) denote the work function differences between the electrodes and the bulk SWNT.

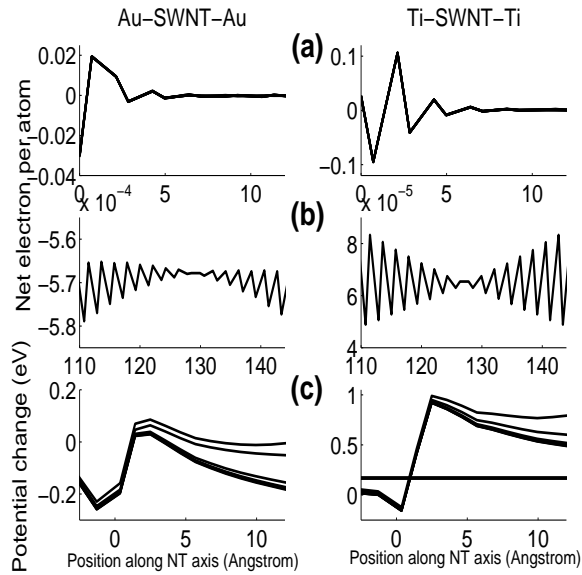


FIG. 3: Magnified view of transferred-charge at the metal-SWNT interface (a) and in the middle of the 60-unitcell SWNT (b). The magnitude of the interfacial charge transfer is approximately identical for all finite SWNTs studied. (c) shows magnified view of the potential shift at the interface.

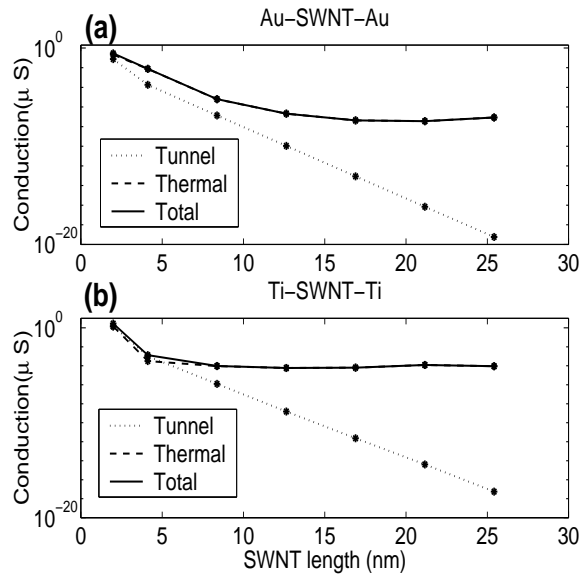


FIG. 4: Room temperature conductance of the metal-finite SWNT-metal junction as a function of SWNT length.